24th COBEM - 2017

24th ABCM International Congress of Mechanical Engineering
December 3-8, 2017, Curitiba, PR, Brazil

COBEM-2017-1180
EXPERIMETAL VERIFICATION OF THE SELF-POWERED ACTIVE CONTROL OF AEROELASTIC OSCILLATIONS USING PIEZOELECTRIC MATERIAL

Douglas D'Assunção
Tarcísio M. P. Silva
Marcel A. Clementino
Carlos De Marqui Jr.
São Carlos School of Engineering, University of São Paulo, 400 Trabalhador São-carlense Avenue, São Carlos - SP
douglasdassuncao@usp.br, tarcismarinelli@hotmail.com, marcelclementino@usp.br, demarqui@sc.usp.br

Abstract. *Piezoelectric materials have been used as sensors and actuators in vibration control problems. Recently, piezoelectric transduction has also received great attention for vibration-based energy harvesting. This paper proposes the self-powered active vibration control of a multilayered structure with two piezoceramic layers for scavenging energy, one for sensing and another one for actuation. An electrical circuit that calculates the control signal based on the electrical output of the sensing piezoelectric layer and simultaneously has energy harvesting capabilities is presented. The actuation energy is supplied by the harvested energy, which also powers active elements of the circuit. The performance of the self-powered active flutter controller is discussed.*

Keywords: *piezoelectricity, self-powered active control, energy harvesting, aeroelasticity*

1. INTRODUCTION

The past few decades have seen the use of piezoelectric materials as sensors and/or actuators in vibration control problems. The vibration control techniques using piezoelectric materials include the passive and active ones. Most recently, piezoelectric materials have also been employed in vibration based energy harvesting investigations, converting the wasted vibration energy available in their environment into electrical energy.

The combination of aeroelastic oscillations and transduction mechanisms for converting flow energy into electrical energy has received growing attention over the past few years (Kwon, 2010; Tang and Dowell, 2010; Abdelkefi et al., 2011). In order to investigate an aeroelastic energy harvesting problem for a 2-DOF (degree-of-freedom) typical section, Erturk et al. (2010) presented an experimentally validated lumped-parameter model for a wing-section (airfoil) with piezoceramics attached onto plunge stiffness members using Theodorsen's unsteady aerodynamic model (Theodorsen, 1935).

The literature of aeroelasticity includes the use piezoelectric actuators to actively modify the aeroelastic behavior of lifting surfaces. Heeg (1993) reports the experimentally verified active flutter control of an aeroelastic typical section using piezoceramics as actuators. The experimental linear flutter speed was increased by 20% when the control loop was closed. The control of dynamic aeroelastic phenomena was also demonstrated in the Piezoelectric Aeroelastic Response Tailoring Investigation (PARTI) conducted at NASA Langley transonic tunnel (Mcgown et al., 1998). The authors report an increase of 12% in flutter dynamic pressure as well as 75% reduction in gust bending moment of a composite plate-like wing with 36 piezoceramic patches.

This paper combines simultaneous energy harvesting and active control on multilayered electromechanically coupled structures to obtain a self-powered active vibration control system. The electrical circuit presented by Silva and De Marqui Jr. (2017), is modified and experimentally verified for the self-powered control of flutter oscillations of a two-degrees-of-freedom (2-DOF) typical section setup. In the experimental system, two layers of piezoelectric material combined in parallel connection are used for wind energy harvesting. Another two patches of piezoceramic are employed as sensors, while two piezoelectric patches employed as actuators. An active state feedback control law is designed and an electrical circuit that calculates the control signal based on the electrical output of the sensing piezoelectric layer is presented. The same circuit has energy harvesting capabilities in order to provide the actuation energy and also power active electrical elements of the circuit. The self-powered active controller is employed to suppress aeroelastic oscillations of the typical section at its flutter boundary.

2. THEORICAL BACKGROUND

Figure 1a shows the schematic of a linear 2-DOF typical section. The plunge and pitch DOF are denoted by h and α, respectively. The plunge displacement is measured at the elastic axis, i.e., at point P (positive downward) and the pitch angle is measured about the elastic axis (positive clockwise). In addition, b is the semichord of the airfoil section, x_α is the dimensionless chord-wise offset of the elastic axis from the centroid (C), k_h is the stiffness per length in the plunge DOF, k_α is the stiffness per length in the pitch DOF, d_h is the damping coefficient per length in the plunge DOF, d_α is the damping coefficient per length in the pitch DOF, and U is the airflow speed. In this work, electromechanical coupling is added to the plunge DOF. This way, aeroelastic vibrations of the cantilever beam (plunge spring) dynamically strain the piezoelectric patches employed as sensors and energy harvesting devices. Moreover, piezoelectric actuators are considered in the same DOF. The schematic of the electroaeroelastic section is shown in Fig. 1b.

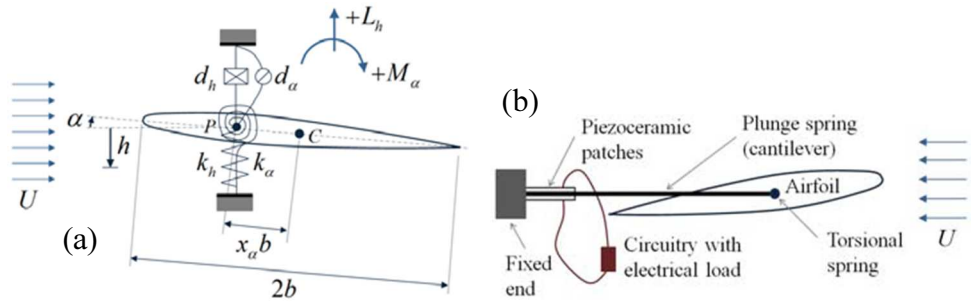

Figure 1. (a) Aeroelastic typical section under airflow excitation; (b) Electroaeroelastic typical section with piezoelectric coupling on the plunge DOF

The equations governing the piezoaeroelastic system are

$$\left(m + m_f\right)\ddot{h} + S_\alpha \ddot{\alpha} + d_h \dot{h} + k_h h - \frac{\theta_1}{l} V_{p1} - \frac{\theta_2}{l} V_{p2} - \frac{\theta_3}{l} V_{p3} = -L \tag{1}$$

$$S_\alpha \ddot{h} + I_\alpha \ddot{\alpha} + d_\alpha \dot{\alpha} + k_\alpha \alpha = M \tag{2}$$

$$V_{p1} + V_c = 0 \tag{3}$$

$$\theta_2 \dot{h} + \frac{V_{p2}}{R_l} + C_{p2}^{eq} \dot{V}_{p2} = 0 \tag{4}$$

$$\theta_3 \dot{h} + \frac{V_{p3}}{R_l} + C_{p3}^{eq} \dot{V}_{p3} = 0 \tag{5}$$

where m is the airfoil mass per length (in the span direction), m_f is the fixture mass (connecting the airfoil to the plunge springs) per length, I_α is the moment of inertia per length about the elastic axis, S_α is the static moment per length, l is the span length, R_l is the load resistance in the electrical domain, V_{pn} is the voltage across the resistive load, C_{pn}^{eq} is the equivalent capacitance of the piezoceramic layers, θ_n is the electromechanical coupling (n=1,2,3), M is the aerodynamic moment per length, L is the aerodynamic lift per length, and the over-dot represents differentiation with respect to time.

The V_c is the control voltage obtained from a Linear Quadratic Regulator (LQR) control law. The piezoaeroelastic system can be represented in state-space, by combining equations (1)-(5) as,

$$\dot{\boldsymbol{x}} = \boldsymbol{A}\boldsymbol{x} + \boldsymbol{B}\boldsymbol{V}_c \tag{6}$$

$$\boldsymbol{Y} = \boldsymbol{C}\boldsymbol{x} \tag{7}$$

$$\boldsymbol{V}_c(t) = -\boldsymbol{K}\boldsymbol{x}(t) = -\{K_1 \;\; K_2 \;\; K_3 \;\; K_4\}\{h \;\; \dot{h} \;\; \alpha \;\; \dot{\alpha}\}^t \tag{8}$$

where $\boldsymbol{x}$ is the state vector, $\boldsymbol{A}$ is the state matrix, $\boldsymbol{B}$ is the control matrix, $\boldsymbol{C}$ is the output matrices, $\boldsymbol{Y}$ is the output vector and $\boldsymbol{K}$ is the optimal control gain so as to minimize the performance index,

$$\boldsymbol{J} = \int_0^T (\boldsymbol{x}^t \boldsymbol{Q} \boldsymbol{x} + \boldsymbol{V}_c^t \boldsymbol{R} \boldsymbol{V}_c) \tag{9}$$

where $\boldsymbol{Q}$ and $\boldsymbol{R}$ are symmetrical and positive matrices chosen arbitrarily (OGATA, 2010). The control gain is presented as:

$$\boldsymbol{K} = \boldsymbol{R}\boldsymbol{B}^t\boldsymbol{P} \tag{10}$$

where $\boldsymbol{P}$ is obtained from Riccati's equation

$$\boldsymbol{A}^t\boldsymbol{P} + \boldsymbol{P}\boldsymbol{A} - \boldsymbol{P}\boldsymbol{B}\bar{\boldsymbol{R}}^{-1}\boldsymbol{B}^t\boldsymbol{P} + \boldsymbol{Q} = \boldsymbol{0} \tag{11}$$

and, therefore, the closed-loop piezoaeroelastic equation for typical section is:

$$\dot{\boldsymbol{x}} = (\boldsymbol{A} - \boldsymbol{B}\bar{\boldsymbol{K}})\boldsymbol{x} \tag{12}$$

2.1 Self-powered control model

The typical section electromechanical coupling is due to three pairs of piezoceramics patches. Each pair accomplishes the function of a haverster, a sensor and actuator. The schematic of the self-powered active control circuit is shown in Fig. 2. Note that V_{p2} is output of the harvester piezoceramic, V_{p3} is output of the sensor piezoceramic and V_c is control voltage applied to the actuator. The V_{p2} output is driven to the rectifier bridge that has a positive and negative half wave rectifier composed by the electrical components D_1, C_1, R_1, D_{z1}, Q_1 and D_2, C_2, R_1, D_{z2}, Q_2, respectively. The harvester circuit powers the operational amplifier (OpAmp) and the actuator circuit.

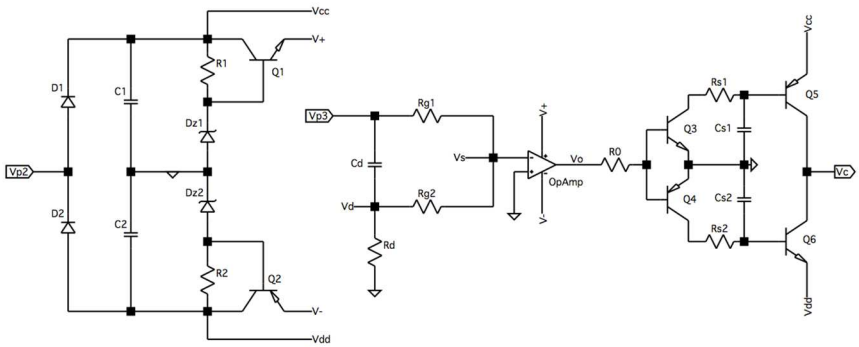

Figure 2. Schematic of the self-powered active control circuit

The sensor circuit presents high impedance, therefore the voltage output of the piezoceramic is defined as,

$$V_{p3} = -\frac{\theta_3 h}{C_{p3}^{eq}} \tag{13}$$

where θ_3 is the electromechanical coupling, C_{p3}^{eq} is the equivalent capacitance of piezoceramic.

Analyzing the sensor circuit (Fig. 2) (Kirchhoff's circuit law), one should obtain,

$$V_s = \left(\frac{R_{G2}}{R_{G1}+R_{G2}}\right)V_{p3} + \left(\frac{R_{G1}}{R_{G1}+R_{G2}}\right)V_D \tag{14}$$

where V_D is

$$V_D = R_D C_D \dot{V}_{p3} = -R_D C_D \frac{\theta_3 \dot{h}}{C_{p3}^{eq}} \tag{15}$$

and the function of resistor R_D and capacitor C_D is to obtain the derivative of voltage V_{p3}.

Therefore the voltage output V_s can be written as

$$V_s = -\left(\frac{R_{G2}}{R_{G1}+R_{G2}}\right)\frac{\theta_3 h}{C_{p3}^{eq}} - \left(\frac{R_{G1}}{R_{G1}+R_{G2}}\right) R_D C_D \frac{\theta_3 \dot{h}}{C_{p3}^{eq}} \tag{16}$$

where V_s is proportional to the displacement and velocity of the structure. This way, V_s must to be in phase and proportional to V_c, as defined by the LQR theory. Therefore combining Eq. (8) and Eq. (16),

$$V_c \approx -K_1 h - K_2 \dot{h} \propto V_s \tag{17}$$

where,

$$K_1 \propto \left(\frac{R_{G2}}{R_{G1}+R_{G2}}\right)\frac{\theta_3}{C_{p3}^{eq}} \tag{18}$$

$$K_2 \propto \left(\frac{R_{G1}}{R_{G1}+R_{G2}}\right) R_D C_D \frac{\theta_3}{C_{p3}^{eq}} \tag{19}$$

which are the gains of the controller.

The voltage output V_0 is a square wave in phase with V_s with amplitudes given by $V_0 = V_+$, if $V_s > 0$ and $V_0 = V_-$, if $V_s < 0$. The voltage V_0 enables an electrical switch composed by the bipolar junction transistors Q_3, Q_4, Q_5 and Q_6. The switch is has three inputs (V_0 V_{cc} and V_{dd}) and one output V_c. When V_0 is positive, Q_3 and Q_5 are turned on, and V_c is connected to V_{cc}. Likewise, when V_0 is negative, Q_4 and Q_6 are turned on, and V_c is connected to V_{dd}.

Therefore,

$$V_c = V_{cc} \text{ if } V_0 > 0 \tag{20}$$

$$V_c = V_{dd} \text{ if } V_0 < 0 \tag{21}$$

and V_c is a square wave with amplitude limited by DC voltages obtained from the rectifier bridge.

3. EXPERIMENTAL SETUP

Figure 3 shows the experimental setup of the linear 2-DOF typical section. The flutter control tests were performed in a blower wind tunnel (test section 0.5 X 0.5 m) with maximum airflow speed of 26 m/s. The plunge stiffness is due to the four elastic cantilevered beams whose free ends are connected to metal plates at the top and bottom of a rigid and symmetric airfoils section, as shown in Fig. 3b. A shaft (that is crosses the quarter chord position of the rigid wing) is mounted to the upper and lower plates though a pair of bearings. The pitch stiffness is given by a spring wire clampled into the shaft and its free end is simply supported on top plate, shown in Fig. 4a. Six piezoceramics patches (QP10N from Mide Technology Corporation), combined into tree pairs, are symmetrically attached onto the root of the bending stiffness members. Each pair comprehended the parallel connection of two PZTs located in the upper and lower beams (Fig. 3b). The actuator was attached on the outter surface of the beam (Fig. 4b), the harvester on the outter surface of the opposite beam (Fig. 4b) and and the sensor on the inner surface of the beam, as indicates Fig. 4c. The properties of the piezoaeroelastic typical section are shown in Table 1.

The plunge displacement (h) is measured using an electrical strain gage bonded on the beam, on a 1/4th bridge configuration, and calibrated to give the beam tip displacement. The pitch displacement (α) is measured with a digital encoder, model HEDS-9000-T00, attached to shaft of the wing. A dSPACE® DS1104 system was used for acquisition of the all data.

Figure 3. (a) Blower wind tunnel, (b) experimental typical section

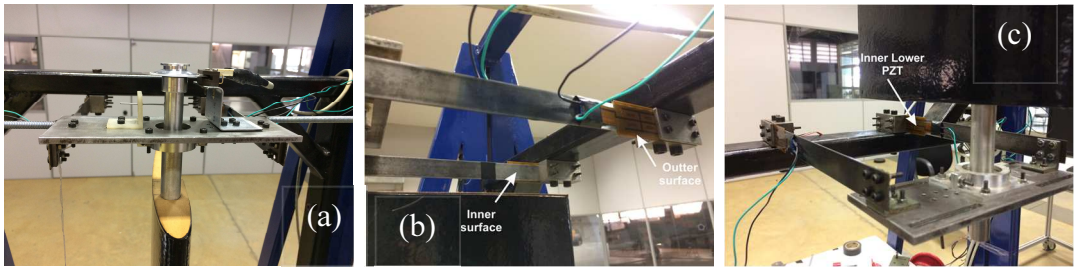

Figure 4. (a) detailed view of the pitch spring (b) detailed view of the piezoceramic on upper beams (c) detailed view of the piezoceramic on lower beams

Table 1. Properties of the aeroelastic typical section.

Parameter	Value	Unit	Description
b	0.125	m	Semichord length
l	0.50	m	Span length
x_α	0.2064	-	Elastic axis distance from midchord (per b)
m	0.780	kg	Rotating mass
m_f	1.091	kg	Translating mass
I_α	0.003	kg·m^2	Moment of inertia
k_α	2.7961	N·m	Pitch DOF stiffness
k_h	2193	N/m	Plunge DOF stiffness
ξ_α	0.014	-	Damping ratio of the pitch DOF
ξ_h	0.078	-	Damping ratio of the plunge DOF
ω_α	30.53	Rad/s	Uncoupled pitch natural frequency
ω_h	34.23	Rad/s	Uncoupled plunge natural frequency
θ_n	1.55 x 10^{-3}	N/V	Electromechanical coupling
C_{pn}^{eq}	95.0	nF	Equivalent capacitance (for each pair of the QP10N patch)

Table 2. Electrical components values employed in the self-powered active circuit.

Component	Value
C_1, C_2	10 uF
C_{s1}, C_{s2}	1 uF
C_D	6.8 nF
D_{Z1}, D_{Z2}	BXZ55C5V6
D_1, D_2	BYW95c
R_D	10 kΩ
R_{s1}, R_{s2}	100 kΩ
R_1, R_2	10 MΩ
R_0	1 MΩ
OpAmp	TVL2211

4. RESULTS AND DISCUSSION

This section examines the experimental feasibility of the self-powered active control of linear aeroelastic responses of the electromechanically coupled 2-DOF typical section described in section 2. The capability of the self-powered system to suppress linear aeroelastic oscillations and to expand the flutter margin is investigated.

First, the short circuit linear flutter speed is experimentally estimated by analyzing time histories of the pitch and plunge DOF. An initial condition (h_0) was applied to the plunge DOF at different airflow speeds and the free oscillation responses observed. If the response of system was stable the airflow speed was increased and an initial condition again applied. This process was repeated until self-sustained oscillations were observed, characterizing the flutter behavior of the typical section.

In the short circuit condition (all piezoelectric elements in short circuit), the electrodes of the three pairs of piezoceramic patches attached onto the root of the bending stiffness are connected to a load resistance $R_l = 100\Omega$. Figure 5 displays the measured time histories of plunge and pitch displacements, with a $h_0 \approx 7.5$ x 10^{-3} m and airflow

speed of 13.8 m/s. The flutter behavior is verified through the self-sustained oscillations and increasing amplitude. For airflow speeds lower than 13.8 m/s the system is stable. Therefore, the airflow speed of 13.8 m/s is assumed as the experimental short circuit flutter speed of the system.

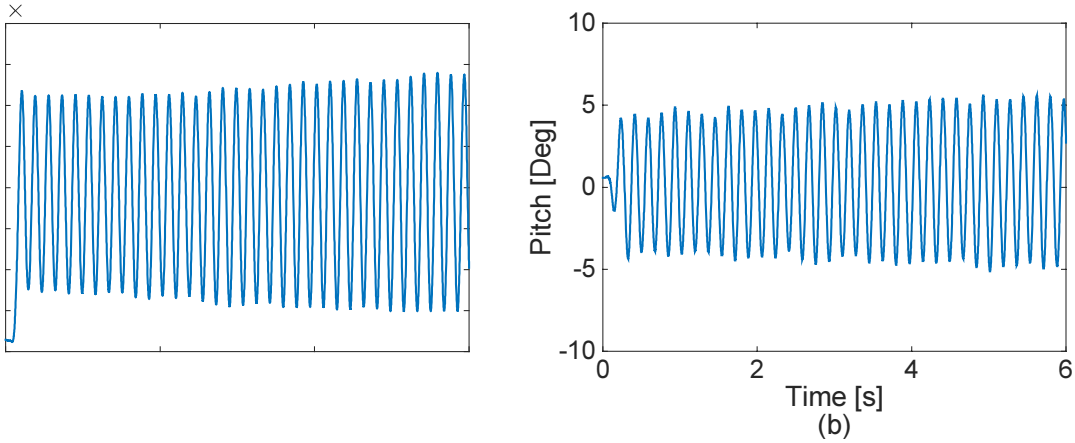

Figure 5. (a) The time histories of plunge displacement, and (b) pitch displacement at airflow speed of the 13.8 m/s

Figure 6 shows the plunge and pitch time histories for the airflow speed of 13.8 m/s when the piezoelements were combined to the self-powered active control circuit of Fig. 2. The self-powered active control system is capable to suppress the linear flutter oscillations at the short circuit flutter speed. Figure 7 shows the harvester voltage output and also the control voltage V_c applied to the piezoelectric actuators.

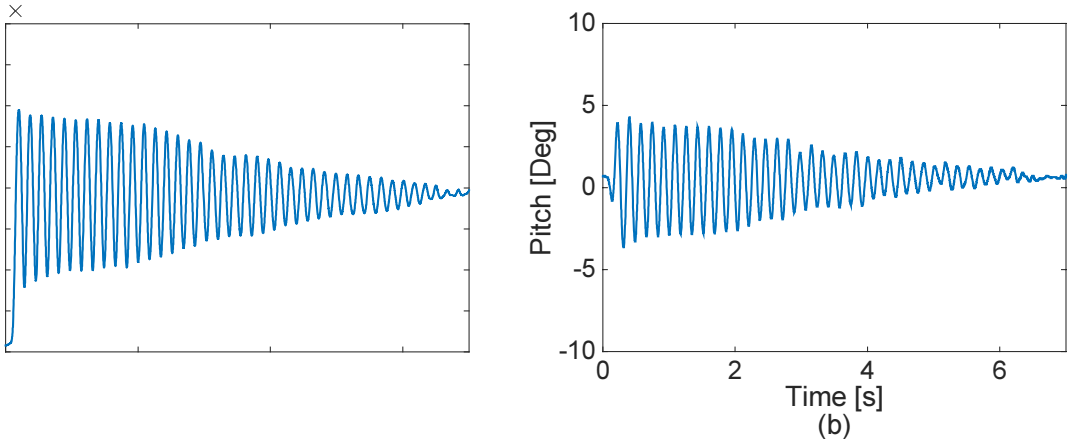

Figure 6. (a) The time histories of plunge displacement, and (b) pitch displacement at airflow speed of the 13.8 m/s

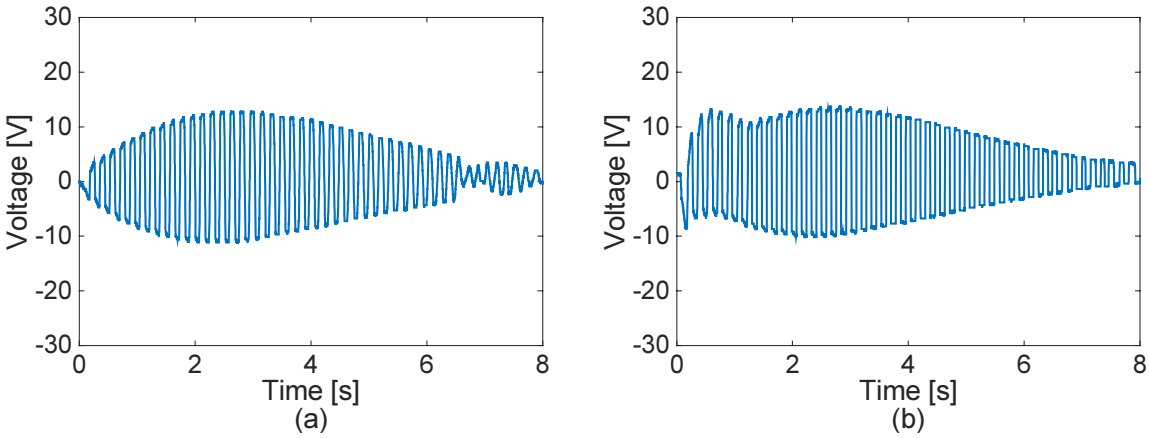

Figure 7. (a) The time histories of harvester voltage, and (b) V_c at airflow speed of the 13.8 m/s

The capability of the self-powered system to expand the flutter margin of the 2-DOF typical section was also experimentally investigated. The flutter oscillations are suppressed for airflow speed smaller than 14.0 m/s. Figure 8 shows unstable plunge and pitch displacements at airflow speed of the 14.0 m/s for the closed loop condition. Therefore, the closed loop flutter speed is 2.0% larger than the short circuit flutter speed Fig. 9 displays the voltage output and also de control voltage for the airflow speed of 14.0 m/s.

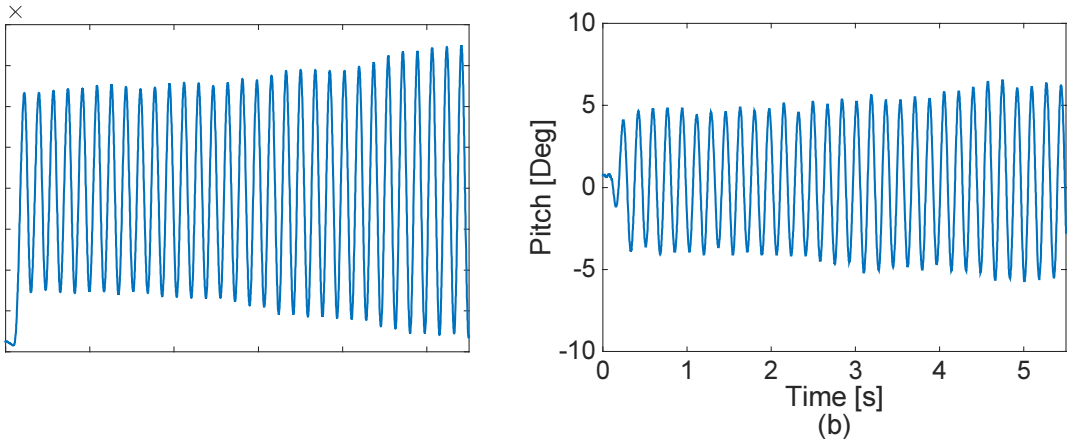

Figure 8. (a) The time histories of plunge displacement, and (b) pitch displacement at airflow speed of the 14.0 m/s

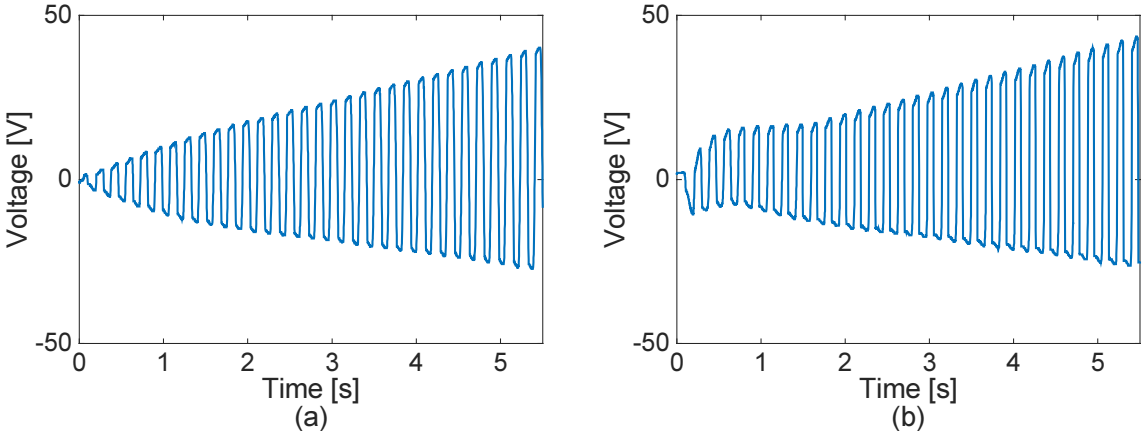

Figure 9. (a) The time histories of harvester voltage, and (b) V_c at airflow speed of the 14.0 m/s

5. CONCLUSIONS

In this paper, self-powered active control of a 2-DOF piezoaerolastic typical section was experimentally investigated. The short circuit linear flutter speed of the typical section was estimated in 13.8 m/s. The self-powered active control system could damp flutter oscillations at the short circuit flutter speed of the system. Moreover, the linear flutter speed of the typical section was increased by 2.0% when using the self-powered active control method. Although the performance of the self-powered control system is limited by the amount of power available for actuation (in the present case, an amount of the harvested energy), this is the first experimental verification of a self-powered active control system (combining wind energy harvesting and active control) presented in the literature.

6. ACKNOWLEDGEMENTS

The authors gratefully acknowledge the support of the CAPES.

7. REFERENCES

Abdelkefi, A., Nayfeh, A. H. and Hajj, M. R., 2011. "Design of piezoaeroelastic energy harvesters". *Nonlinear Dynamics*, v. 68, n. 4, p. 519–530. <http://link.springer.com/10.1007/s11071-011-0233-x>.

Erturk, A., Vieira, W. G. R., De Marqui, C. and Inman, D. J., 2010. "On the energy harvesting potential of piezoaeroelastic systems". *Applied Physics Letters*, v. 96, n. 18, p. 184103, 2010.

Heeg, J., 1993. "Analytical and Experimental Investigation of Flutter Suppression by Piezoelectric Actuation". *NASA Technical Paper 3241*.

Kwon, S.-D., 2010. "T-shaped piezoelectric cantilever for fluid energy harvesting". *Applied Physics Letters*, v. 97, n. 16, p. 164102.

Mcgowan, A., Wilkie, W. K., Moses, R. W., et al., 1998. "Aeroservoelastic and structural dynamics research on smart structures conducted at NASA Langley Research Center". *Proceedings of SPIE - The International Society for Optical Engineering*. v. 3326, p.188–201.

OGATA, K. *Modern Control Engineering.* Fifth Edit ed. Upper Saddle River: Pearson/Prentice Hall, 2010.

Silva, T. M. P. and De Marqui, C., 2017. "Self-powered active control of elastic and aeroelastic oscillations using piezoelectric material". *Journal of Intelligent Material Systems and Structures*, v. 28, n. 15, p. 2023–2035. <http://journals.sagepub.com/doi/10.1177/1045389X16685448>.

Tang, D. and Dowell, E. H., 2010. "Aeroelastic airfoil with free play at angle of attack with gust excitation". *AIAA Journal*, v. 48, n. 2, p. 427–442.

Theodorsen, T., 1935. "General theory of aerodynamics instability and the mechanism of flutter", n. 496.

8. RESPONSIBILITY NOTICE

The authors are the only responsible for the printed material included in this paper.